PCCP

Accepted Manuscript

ROYAL SOCIETY OF CHEMISTRY

www.rsc.org/pccp

Blue absorption and red emission of Bi^{2+} in solids: strongly spin-orbit coupled $6p$ levels in low symmetry fields.

Luis Seijo[1,2,*] and Zoila Barandiarán[1,2]

[1]*Departamento de Química, Universidad Autónoma de Madrid, 28049 Madrid, Spain*

[2]*Instituto Universitario de Ciencia de Materiales Nicolás Cabrera, Universidad Autónoma de Madrid, 28049 Madrid, Spain*

Abstract

Wave function embedded cluster *ab initio* calculations on a $(BiO_8)^{14-}$ cluster under the effects of a high symmetry O_h confinement potential are used to study the energies of the $^2P_{1/2}$, $^2P_{3/2}(1)$, and $^2P_{3/2}(2)$ spin-orbit coupling levels of the $6s^26p$ configuration of Bi^{2+} in O_h, D_{4h}, D_{2h}, D_4, D_{2d}, D_2, S_4, C_{4v}, C_4, C_{3v}, C_{2v}, C_2, C_s, and C_1 fields, together with the $^2P_{1/2} \rightarrow ^2P_{3/2}(1)$ and $^2P_{1/2} \rightarrow ^2P_{3/2}(2)$ absorption oscillator strengths and $^2P_{3/2}(1)$ radiative lifetime. These levels are responsible for the blue absorptions and the red-orange emissions produced when Bi^{2+} is doped in borates, phosphates, sulphates, and other hosts. It is found that the splitting of $^2P_{3/2}$ is mainly due to the tetragonal D_{4h} and orthorhombic D_{2h} components of the actual field. It is enhanced by Bi going towards two or four ligands. The intensities of the $^2P_{1/2} \rightarrow ^2P_{3/2}(1)$ and $^2P_{1/2} \rightarrow ^2P_{3/2}(2)$ absorptions are mostly induced by the Bi displacements and by tetragonal scalenoidal D_{2d} fields. The most favorable fields for a large splitting of the $^2P_{3/2}$ level that could drive a red shift of the $^2P_{3/2}(1) \rightarrow ^2P_{1/2}$ emission are the C_{2v} and C_s fields resulting from the combination of D_{2h} orthorhombic fields and Bi approaching two or four ligands on the main orthorhombic planes.

Keywords: *Ab initio*, bismutsh, Bi^{2+}, spin-orbit coupling, low symmetry fields, red emission, blue absorption

I. INTRODUCTION

The Bi^{2+} ion has recently motivated a new line of approach in the search of new red phosphors for energy efficient solid-state lighting devices.[1–7] This line finds its grounds on the earlier work of Blasse *et al.*,[8] who considered the rarely reported divalent bismuth species as responsible for the red-orange luminescence of bismuth activated SrB_4O_7. By extension, Bi^{2+} was assumed to cause the red luminescence of bismuth activated alkaline earth sulfates already reported in 1886 by Lecoq de Boisbaudran[9] and of bismuth activated phosphates reported in 1949 by Kröger *et al.*[10] (cf. Ref. 11).

What makes this ion attractive for blue-LED based white light illuminating devices is the fact that it has a red-orange emission band at around 17000 cm^{-1} that can be excited with blue light at around 21000 cm^{-1} in borates, sulfates, and phosphates,[1,3,8] and both the excitation and the emission are in principle susceptible to being tailored by selection of the hosts. These electronic transitions have been interpreted as $6p \rightarrow 6p$ parity forbidden transitions between local states associated with the spin-orbit $^2P_{1/2}$ and $^2P_{3/2}$ levels of the $6s^2 6p$ configuration of Bi^{2+}.[1,3,8] The low symmetry fields acting on the Bi^{2+} ion in the solid hosts are responsible for: (1) the splitting of $^2P_{3/2}$ into two $^2P_{3/2}(1)$ and $^2P_{3/2}(2)$ levels, which enables a $^2P_{1/2} \rightarrow ^2P_{3/2}(2)$ excitation and a $^2P_{3/2}(1) \rightarrow ^2P_{1/2}$ emission, and (2) the breaking of the electric dipole selection rule, which makes both transitions allowed and gives a finite value to the $^2P_{3/2}(1)$ radiative lifetime (12.6 μs in SrB_4O_7:Bi^{2+} [Refs. 2,7,8,12]).

Wave-function-based embedded-cluster *ab initio* calculations on Bi^{2+}-doped SrB_4O_7 have been shown to be reliable enough so as to help interpreting its electronic structure[7] and its vibrational structure.[13] Although such calculations are far from routine and they are time consuming, they can in principle be performed in other Bi^{2+}-doped hosts in a one-by-one basis. Nevertheless, as in the case of Ce^{3+}-doped garnets,[14,15] we can expect the relevant level energies and wave functions of Bi^{2+} in solids with oxygen coordination to be dominated, up to first-order, by the bonding interactions between Bi and its first oxygen coordination shell, subject to the basic confinement embedding effects of the host, whereas other specific host embedding effects are important at higher orders of approximation and they will refine the results. Then, an *ab initio* calculation of a cluster of Bi^{2+} and its oxygen coordination shell under the effects of a high symmetry confinement potential should provide the basics of the $^2P_{1/2}$, $^2P_{3/2}(1)$, and $^2P_{3/2}(2)$ levels.

On the basis of such idea, we report in this paper a basic *ab initio* study of the energies of the $^2P_{1/2}$, $^2P_{3/2}(1)$, and $^2P_{3/2}(2)$ levels of the $6s^26p$ configuration of Bi^{2+} in low symmetry fields created by oxygen coordinations, of the two absorption oscillator strengths, and of the radiative lifetime of the emitting, first excited state. We explored fields of O_h, D_{4h}, D_{2h}, D_4, D_{2d}, D_2, S_4, C_{4v}, C_4, C_{3v}, C_{2v}, C_2, C_s, and C_1 symmetries. The results are expected to be helpful in the search for new hosts for Bi^{2+} with tailored blue absorptions and red emissions.

II. METHOD

The *ab initio* calculations in this paper are designed to study the splitting of the $^2P_{1/2}$ and $^2P_{3/2}$ atomic levels of the $6s^26p$ configuration of Bi^{2+} in a number of low symmetry fields that could be found in solids where Bi^{2+} occupied a site with a first coordination shell of oxygens. These energy levels are responsible for the blue absorptions and the red emissions of the Bi^{2+}-doped solids and, accordingly, we not only calculated their energies but also the corresponding absorption oscillator strengths and emitting state radiative lifetimes.

Here we study low symmetry fields originated by arbitrary atomic displacements within a $(BiO_8)^{14-}$ cluster. Although 9-fold oxygen coordination has been found for Bi^{2+} in some solids,[8] the 8-fold coordinated cluster allows us to start from a high symmetry (O_h) that serves as a reference for all level splittings. Besides, the $6p \rightarrow 6p$ transitions are forbidden in this highly symmetric reference, so that it is also useful to see the origin of the absorption intensities and of the limited lifetime of the emitting state. We expect the symmetry and strength of the effective field generated by the oxygen ligands, rather than their number, to be the main factor dominating these transitions.

We embedded the $(BiO_8)^{14-}$ cluster in a O_h host potential that was kept constant in all the calculations. In this way, the embedding potential contributes electrostatic and quantum (exchange and Pauli repulsion) interactions with the host, which are important to confine the electrons in the local region around Bi^{2+}, and it provides a high symmetry environment, so that all the low symmetry effects are ascribable to the interactions between Bi and its first oxygen coordination shell.

The quantum mechanical calculation have been performed with the MOLCAS suite of programs.[16] In brief, these are AIMP embedded cluster SA-CASSCF/MS-CASPT2/RASSI-SO DKH calculations. They include Bi-O bonding effects, static and dynamic electron correlation ef-

fects, scalar and spin-orbit coupling relativistic effects, and cubic host embedding effects. The details are the following: For each nuclear configuration of the $(BiO_8)^{14-}$ embedded cluster, we performed, in a first step, scalar relativistic calculations with the many-electron second-order Douglas-Kroll-Hess (DKH) Hamiltonian.[17,18] These were state-average complete-active-space self-consistent-field[19–21] (SA-CASSCF) calculations with the active space that results from distributing 3 electrons in 3 active molecular orbitals with main character Bi $6s, 6p$, which provided occupied and empty molecular orbitals to feed subsequent multi-state second-order perturbation theory calculations (MS-CASPT2),[22–25] where the dynamic correlation of 77 electrons have been taken into account (the $5d, 6s, 6p$ electrons of Bi and $2s, 2p$ electrons of the O atoms). We used the standard IPEA value (0.25 au).[26] In a second step, we included spin-orbit coupling effects by adding the AMFI approximation of the DKH spin-orbit coupling operator[27] to the scalar relativistic Hamiltonian. In this step, we used the spin-free-state-shifting operator as a means to combine spin-orbit couplings calculated with statically correlated wave functions and spin-orbit free energies calculated with dynamic correlation[28] and, accordingly, we performed restricted-active-space state-interaction spin-orbit calculations (RASSI-SO)[29,30] with the transformed CASSCF wave functions (first-order wave functions of the MS-CASPT2 method) and the MS-CASPT2 energies. All the calculations are all-electron, with atomic natural orbital (ANO) relativistic basis sets for bismuth and oxygen,[31] with respective contractions $(25s22p16d12f4g)/[11s10p9d6f4g]$ and $(14s9p4d)/[4s3p2d]$.

In all these calculations, the Hamiltonian of the $(BiO_8)^{14-}$ cluster was supplemented with a cubic embedding Hamiltonian that was previously used in a study of the $4f$ and $5d$ levels of Ce^{3+} in D_2 8-fold oxygen coordination.[14] It is the *ab initio* model potential embedding Hamiltonian (AIMP)[32] of a SrO host in its high pressure CsCl lattice structure[33] ($Pm\bar{3}m$, no. 221), which provides a perfect 8-fold cubic oxide coordination of the cationic site. The embedding potential of this 8-fold coordinated cubic oxide was computed with a lattice constant $a = 2.87$ Å, in Hartree-Fock self-consistent embedded-ions calculations (SCEI),[34] in which the input embedding AIMPs used for the Sr^{2+} and O^{2-} ions of SrO are consistent with the output AIMPs obtained out of the HF orbitals of the embedded Sr^{2+} and O^{2-} ions.

The effective fields of different symmetries have been generated by means of coordinated displacements of the oxygen and the bismuth atoms of the BiO_8 moiety. The chosen basic distortions of the BiO_8 reference cube are defined in Table I and shown in Figs. 1 and 2. Note that the energies are invariant under sign change of the distortions S_3 to S_8.

Combinations of the basic distortions lead to lower symmetries. The specific combinations of basic distortions chosen in this work and the symmetry fields they produce are listed in Table II. Their graphical representations are included in Figs. 3 to 7. The minimum Bi-O and O-O distances reached with the explored distortions represented in these figures are also shown in Table II in order to give an idea of the size of the distortions.

The electronic states under consideration are usually labeled $^2P_{1/2}$, $^2P_{3/2}(1)$, and $^2P_{3/2}(2)$, in reference to their main free-ion characters. At the spin-orbit coupling level considered here, all of them are Kramers doublets. The previous notation is convenient and we will use it in the discussion (Sec. III). In the O_h group they are labeled $1E_{1/2,u}$ and $1G_{3/2,u}$, the last one with additional double degeneracy. In D_{4h} they are $1E_{1/2,u}$, $2E_{1/2,u}$, and $1E_{3/2,u}$; in D_{2h}, $1E_{1/2,u}$, $2E_{1/2,u}$, and $3E_{1/2,u}$; in D_4, $1E_{1/2}$, $2E_{1/2}$, and $1E_{3/2}$; and in all other groups studied here they are $1E_{1/2}$, $2E_{1/2}$, and $3E_{1/2}$.

The electronic absorption oscillator strengths have been calculated as:[35,36]

$$f_{\text{abs}}(a \rightarrow b) = \frac{2}{3} \Delta E_{ab} \mu_{ab}^2, \tag{1}$$

where a stands for the ground level $^2P_{1/2}$ and b for the final level, either $^2P_{3/2}(1)$ or $^2P_{3/2}(2)$. ΔE_{ab} is the electronic transition energy, in hartree (1 hartree = 219474.625 cm^{-1}) and μ_{ab}^2 is defined in terms of the electric dipole transition moments (in au) between one of the two degenerate states γ_a of the ground level and the two degenerate states γ_b of the final, excited level:

$$\mu_{ab}^2 = \sum_{\gamma_b=1}^{2} |\langle a\,\gamma_a \,|\, \hat{\mu} \,|\, b\,\gamma_b \rangle|^2. \tag{2}$$

The lifetime for spontaneous emission from the first excited level $^2P_{3/2}(1)$, τ_{rad}, is $\tau_{rad} = 1/A_{ab}$, where b stands for $^2P_{3/2}(1)$ and a for the ground level $^2P_{1/2}$, which is the only one below the emitter. The Einstein coefficient for spontaneous emission is calculated as:[35,36]

$$A_{ab} = \frac{2\,\omega_{ab}^3\,\mu_{ab}^2}{3\,\epsilon_o\,h\,c^3} = \frac{16\,\pi^3\,\mu_{ab}^2}{3\,\epsilon_o\,h\,\lambda_{ab}^3}, \tag{3}$$

where ω_{ab} is the emission angular frequency, $\omega_{ab} = 2\pi c/\lambda_{ab}$, λ_{ab} is the emission wavelength, h is Planck's constant, c the velocity of light, and ϵ_o the permittivity of vacuum. No local field corrections have been included.[37] If ΔE_{ab} is expressed in cm^{-1} and μ_{ab} in au, the expression for A_{ab} in s^{-1} becomes: $A_{ab} = 2.02608 \times 10^{-6} \Delta E_{ab}^3\,\mu_{ab}^2$ (Ref. 35).

III. RESULTS

The results of the energies of the excited states $^2P_{3/2}(1)$ and $^2P_{3/2}(2)$ relative to the ground state $^2P_{1/2}$, the corresponding first and second absorption electric dipole oscillator strengths, $f_{\rm abs}(^2P_{1/2} \rightarrow^2 P_{3/2}(1))$ and $f_{\rm abs}(^2P_{1/2} \rightarrow^2 P_{3/2}(2))$, and the emitting state $^2P_{3/2}(1)$ radiative lifetime $\tau_{\rm rad}$, are shown in Figs. 3 to 7 for fields of different symmetries.

Fig. 3 shows that the energies of the excited degenerate $^2P_{3/2}$ levels in O_h symmetry are only very slightly dependent on the strength of the field. The tetragonal D_{4h} and orthorhombic D_{2h} fields can provide large splittings of $^2P_{3/2}(1)$ and $^2P_{3/2}(2)$, even though they do not give any intensity to the absorptions and the emission. These splittings corresponds to a $G_{3/2} \otimes e_g$ Jahn-Teller coupling between a $G_{3/2,u}$ doubly degenerate spin-orbit coupling level (apart from Kramers degeneracy) and a doubly degenerate e vibration. This vibronic coupling is isomorphous with the well known $E \otimes e_g$ Jahn-Teller coupling problem[38] between an E doubly degenerate level and the doubly degenerate e_g vibration. The fact that the splittings observed in the two D_{4h} and D_{2h} fields are very similar indicates that the Jahn-Teller coupling experienced by Bi^{2+} matches the linear JT coupling limit very well, leading to an almost perfect Mexican hat type of $G_{3/2} \otimes (e_g\theta + e_g\epsilon)$ energy surfaces,[38] without significant energy barriers connecting the three equivalent D_{4h} minima. This is even more clear in Fig. 11 of the Supplementary Material, where cross sections of these surfaces along the $e_g\theta$ and $e_g\epsilon$ vibrational coordinates are shown.

In Fig. 3 we also observe that the tetragonal trapezoidal D_4 and the tetragonal scalenoidal D_{2d} fields created by the $e_u\theta$ and $e_u\epsilon$ deformations S_4 and S_5, do not produce significant $^2P_{3/2}$ splittings. Note that these vibrations are not Jahn-Teller active for the $G_{3/2,u}$ states (cf. Fig. 12 of Supplemental Material). The D_{2d} field gives relevant intensity to the transitions, but the D_4 field does only give a negligible amount, even when it is as intense as in garnets. [The $S_4(e_u\theta)$ and $S_5(e_u\epsilon)$ distortions defined here coincide with the $S_5(e_u\theta)$ and $S_6(e_u\epsilon)$ distortions of the $(CeO_8)^{13-}$ cluster in D_2 sites of garnets used in Refs. 14 and 15, where the value of the $e_u\theta$ distortion was found to lie between 0.95 and 1.09 Å in 21 different garnets and the value of the $e_u\epsilon$ distortion between -0.2 and 0.1 Å.]

Effects of fields resulting from combinations of two S_2-S_5 deformations are shown in Fig. 4. A combination of S_2 and S_3 gives basically the same results as the individual S_2 or S_3, in correspondence with the topology of the Mexican hat energy surface, and it is not shown in the

Figure. The D_2 field resulting from combining S_4 and S_5 gives a very small splitting of $^2P_{3/2}$, as expected from the individual distortions, together with intensities that correspond to S_5 alone. The combinations of S_2-S_3 with S_4-S_5 lead to C_4, S_4, D_2, and C_{2v} fields. Regardless of their symmetry, all of them give important splittings, which are originated by the contributions of the two former e_g individual distortions, S_2 or S_3. Only the D_2, S_4, and C_{2v} fields with contributions from S_5 give relevant intensities; the intensities in D_2 and C_4 fields from combining S_2-S_3 with S_4 are negligible. It is clear that it is not the symmetry of the field, but the contributions behind it, what are responsible for the splitting of $^2P_{3/2}$ and for the intensities of the $^2P_{1/2} \rightarrow^2 P_{3/2}(1)$ and $^2P_{1/2} \rightarrow^2 P_{3/2}(2)$ transitions.

The previous fields basically sample different angular distributions of the coordination shell of Bi^{2+}, with small variations of Bi-O distances. In Fig. 5 we show the effects of C_{4v}, C_{3v}, C_{2v}, C_s, and C_1 fields due to selective changes of Bi-O distances. They also contain some ligand angular distribution effects, though. It is interesting to see that the $^2P_{3/2}$ splitting and emitting state lifetime show similar behaviors in all these fields, no matter if Bi^{2+} approaches one, two, or four oxygen atoms. This suggests that the components of the basic splitting enabling fields are similar in all cases. The relative values of the first and second absorption oscillator strengths are more sensitive to the symmetry of field during the approach of Bi^{2+} to the ligands: the second absorption is more intense in C_{3v}, C_{2v}, and C_1 fields, the first one in C_{4v}, and they are similar in C_s. In summary, the movement of Bi^{2+} towards the ligands creates relevant splittings and rises the oscillator strengths; it is less efficient than the D_{4h} and D_{2h} tetragonal distortions at splitting the $^2P_{3/2}$ level, and as efficient as the D_{2d} tetragonal deformations at giving intensity to the $^2P_{1/2} \longleftrightarrow^2 P_{3/2}$ transitions.

Combined effects of ligand angular distributions and selective Bi-O distance changes are shown in Figs. 6 to 9. In Fig. 6 we see that the combination of the D_{4h} tetragonal distortion with a Bi displacement along the C_4 axis, leading to a $C_{4v}(z)$ field, give a complicated behavior, which is not shown in any other combination. It is the result of a balance of positive and negative contributions of the same type: The effect of S_8 (positive and negative) on the level splitting is the same than the effect of compressed D_{4h} distortions produced by negative S_2 values. It is, however, opposite to the effect of elongated D_{4h} distortions produced by positive S_2 values. As a result, whereas elongated and compressed D_{4h} fields split $^2P_{3/2}$ equally, only the compressed D_{4h} field is effective if Bi is displaced along the C_4 axis. For other displacements of Bi, the effectiveness of elongated and compressed D_{4h} fields are similar.

Fig. 7 shows that the splittings of $^2P_{3/2}$ produced by D_{2h} orthorhombic fields are added to the splittings due to Bi displacements towards the ligands when these take place without leaving the main orthorhombic planes and lead to C_{2v} and C_s fields. This is not the case when Bi abandons the orthorhombic main planes to give a C_1 field. Figs. 8 and 9 indicate that the combinations of tetragonal trapezoidal D_4 and tetragonal scalenoidal D_{2d} fields do not enhance the splittings due to Bi approaching the ligands.

The overall results show that a large splitting of the $^2P_{3/2}$ level that could drive a red shift of the $^2P_{3/2}(1) \rightarrow ^2P_{1/2}$ emission is not associated with the symmetry of the actual field. The low symmetry of the field is not particularly relevant for the splitting: many C_1 fields do not lead to an important splitting and C_s fields can give either small or large splittings. The same happens with higher symmetry fields, like C_{2v}, C_4, C_{4v}, or D_2. Some high symmetry fields give relevant splittings, like S_4, D_{2h}, and D_{4h}, and some do not, like D_4 and D_{2d}. The important factor is the composition of the actual field. All fields with tetragonal D_{4h} and orthorhombic D_{2h} contributions give important $^2P_{3/2}$ splittings. They are enhanced by selective approaches of Bi to the ligands. These Bi displacements and tetragonal scalenoidal D_{2d} fields give intensities to the first and second absorptions.

The results also indicate that the low symmetry fields that break the parity rule and make the present $6p \rightarrow 6p$ transitions allowed, give an upper limit to the oscillator strengths in the order of 10^{-4}-10^{-3}. Similarly, radiative lifetimes of $^2P_{3/2}(1)$ seem to be bound by a lower limit of around 10-100 μs.

The C_{2v} and C_s fields resulting from the combination of D_{2h} orthorhombic fields and Bi displacements towards the ligands on the main orthorhombic planes produce the largest $^2P_{3/2}$ splittings (cf. Fig. 7). They do not have oscillator strengths and emitting state lifetimes specially different from other fields.

A recent *ab initio* study of SrB_4O_7:Bi^{2+} using the SrB_4O_7 embedding potential, which contains not only the first-neighbor field effects considered here but also the host effects, gave a $^2P_{3/2}$ splitting as large as 7200 cm^{-1} (3460 cm^{-1} experiment[2,7,12]), first and second absorption oscillator strengths of 4×10^{-4} and 1×10^{-3}, and a $^2P_{3/2}(1)$ radiative lifetime of 17 μs without field corrections (experiment is 12.6 μs[2,7,8,12]). In this material Bi^{2+} occupies a C_s Sr site with 9-fold oxygen coordination[39] (Fig. 10). This result seems to fit well with the C_s field resulting from the D_{2h} orthorhombic field created by a $S_3(e_g\epsilon)$ distortion plus an approach of Bi towards two or four ligands. Emission lifetimes in the range of 6-17 μs have been reported

for Bi^{2+} in $CaSO_4$, $SrSO_4$, and $BaSO_4$ (Refs. 2, 40), and in $Sr_2P_4O_7$ and $Ba_2P_4O_7$ (Refs. 3,41). In $Ba_2P_4O_7$, the oscillator strength of the $^2P_{1/2} \rightarrow^2 P_{3/2}(1)$ absorption has been estimated to be as large as 0.03.[41]

IV. CONCLUSIONS

SA-CASSCF/MS-CASPT2/RASSI-SO DKH wave function *ab initio* calculations on a $(BiO_8)^{14-}$ cluster under the effects of an O_h confinement embedding potential have provided the energies of the $^2P_{1/2}$, $^2P_{3/2}(1)$, and $^2P_{3/2}(2)$ spin-orbit coupling levels of the $6s^26p$ configuration of Bi^{2+} in O_h, D_{4h}, D_{2h}, D_4, D_{2d}, D_2, S_4, C_{4v}, C_4, C_{3v}, C_{2v}, C_2, C_s, and C_1 fields created by oxygen coordination, together with the $^2P_{1/2} \rightarrow^2 P_{3/2}(1)$ and $^2P_{1/2} \rightarrow^2 P_{3/2}(2)$ absorption oscillator strengths and $^2P_{3/2}(1)$ radiative lifetime.

The results indicate that it is not the symmetry of the actual field, but its tetragonal D_{4h} and orthorhombic D_{2h} components, what are responsible for the splitting of $^2P_{3/2}$. Bi going towards two or four oxygen ligands enhances the splitting. The intensities of the first and second absorptions are mostly induced by these Bi displacements and by tetragonal scalenoidal D_{2d} fields.

The most favorable fields for a large splitting of the $^2P_{3/2}$ level that could drive a red shift of the $^2P_{3/2}(1) \rightarrow^2 P_{1/2}$ emission in oxygen coordination are the C_{2v} and C_s fields resulting from the combination of D_{2h} orthorhombic fields and Bi approaching two or four ligands on the main orthorhombic planes.

---

* Corresponding author; Electronic address: luis.seijo@uam.es

[1] A. M. Srivastava, J. Lumin. **78**, 239 (1998).

[2] M. Peng and L. Wondraczek, Opt. Lett. **34**, 2885 (2009).

[3] M. Peng and L. Wondraczek, Opt. Lett. **35**, 2544 (2010).

[4] Z. Bai, M. Fujii, T. Hasegawa, S. Kitano, K. Imakita, M. Mizuhata, and S. Hayashi, Opt. Mater. **34**, 821 (2012).

[5] M. Peng, J. Lei, L. Li, L. Wondraczek, Q. Zhang, and J. Qiu, J. Mater. Chem. C **1**, 5303 (2013).

[6] R. Cao, F. Zhang, C. Liao, and J. Qiu, Opt. Express **21**, 15728 (2013).

[7] M. de Jong, A. Meijerink, Z. Barandiarán, and L. Seijo, J. Phys. Chem. C **118**, 9696 (2014).

[8] G. Blasse, A. Meijerink, M. Nomes, and J. Zuidema, J. Phys. Chem. Solids **55**, 171 (1994).

[9] F. Lecoq de Boisbaudran, C. R. Acad. Sci. Paris **103**, 629 (1886).

[10] F. A. Kröger, J. T. G. Overbeek, J. Goorissen, and J. van den Boomgaard, Trans Electrochem. Soc. **96**, 132 (1949).

[11] M. A. Hamstra, H. F. Folkerts, and G. Blasse, J. Mater. Chem. **4**, 1349 (1994).

[12] G. Blasse and A. Bril, J. Chem. Phys. **47**, 5139 (1967).

[13] M. de Jong, A. Meijerink, Z. Barandiarán, and L. Seijo, submitted to J. Phys. Chem. C, under revision.

[14] L. Seijo and Z. Barandiarán, Opt. Mater. **35**, 1932 (2013).

[15] L. Seijo and Z. Barandiarán, Phys. Chem. Chem. Phys. **15**, 19221 (2013).

[16] G. Karlström, R. Lindh, P. A. Malmqvist, B. O. Roos, U. Ryde, V. Veryazov, P. O. Widmark, M. Cossi, B. Schimmelpfennig, P. Neogrady, et al., Comput. Mater. Sci. **28**, 222 (2003).

[17] M. Douglas and N. M. Kroll, Ann. Phys. (N.Y.) **82**, 89 (1974).

[18] B. A. Hess, Phys. Rev. A **33**, 3742 (1986).

[19] B. O. Roos, P. R. Taylor, and P. E. M. Siegbahn, Chem. Phys. **48**, 157 (1980).

[20] P. E. M. Siegbahn, A. Heiberg, B. O. Roos, and B. Levy, Phys. Scr. **21**, 323 (1980).

[21] P. E. M. Siegbahn, A. Heiberg, J. Almlöf, and B. O. Roos, J. Chem. Phys. **74**, 2384 (1981).

[22] K. Andersson, P.-A. Malmqvist, B. O. Roos, A. J. Sadlej, and K. Wolinski, J. Phys. Chem. **94**, 5483 (1990).

[23] K. Andersson, P.-A. Malmqvist, and B. O. Roos, J. Chem. Phys. **96**, 1218 (1992).

[24] A. Zaitsevskii and J.-P. Malrieu, Chem. Phys. Lett. **233**, 597 (1995).

[25] J. Finley, P.-A. Malmqvist, B. O. Roos, and L. Serrano-Andrés, Chem. Phys. Lett. **288**, 299 (1998).

[26] G. Ghigo, B. O. Roos, and P.-A. Malmqvist, Chem. Phys. Lett. **396**, 142 (2004).

[27] B. A. Hess, C. M. Marian, U. Wahlgren, and O. Gropen, Chem. Phys. Lett. **251**, 365 (1996).

[28] R. Llusar, M. Casarrubios, Z. Barandiarán, and L. Seijo, J. Chem. Phys. **105**, 5321 (1996).

[29] P. A. Malmqvist, B. O. Roos, and B. Schimmelpfennig, Chem. Phys. Lett. **357**, 230 (2002).

[30] J. Paulovic, T. Nakajima, K. Hirao, R. Lindh, , and P.-A. Malmqvist, J. Chem. Phys. **119**, 798 (2003).

[31] B. O. Roos, R. Lindh, P. A. Malmqvist, V. Veryazov, and P. O. Widmark, J. Phys. Chem. A **108**, 2851 (2005).

[32] Z. Barandiarán and L. Seijo, J. Chem. Phys. **89**, 5739 (1988).

[33] Y. Sato and R. Geanioz, J. Geophys. Res. **86**, 11773 (1981).

[34] L. Seijo and Z. Barandiarán, J. Chem. Phys. **94**, 8158 (1991).

[35] J. Oddershede, Phys. Scr. **20**, 587 (1979).

[36] R. C. Hilborn, Am. J. Phys. **50**, 982 (1982).

[37] D. Toptygin, J. Fluoresc. **13**, 201 (2003).

[38] I. B. Bersuker, *The Jahn-Teller Effect and Vibronic Interactions in Modern Chemistry* (Plenum Press, New York and London, 1984).

[39] J. Krogh-Moe, Acta Chem. Scand. **18**, 2055 (1964).

[40] R. Cao, M. Peng, and J. Qiu, Opt. Express **20**, A977 (2013).

[41] M. Peng, B. Sprenger, M. A. Schmidt, H. G. L. Schwefel, and L. Wondraczek, Opt. Express **18**, 12852 (2010).

TABLE I: Definitions of the basic distortions of a cubic BiO_8 moiety chosen in this work. The oxygen labels and the cartesian axes are defined in Fig. 1. $\hat{R}_{D_{2h}}$ and $\hat{R}_{D_2}$ are the D_{2h} and D_2 symmetrization operators: the normalized additions of the respective group symmetry operations. δx_1, δy_1, and δz_1, are the cartesian displacement of O_1 from its position in the reference cube: $\delta x_1 = x_1 - x_{1,\mathrm{ref}}$, etc. The O_h irreducible representations of the coordinates and the point symmetry groups of the BiO_8 moiety after the atomic displacements of the individual coordinates are given. The reference cube has d(Bi-O)=2.55 Å.

$$\hat{R}_{D_{2h}} = \frac{1}{\sqrt{8}}\left(\hat{I} + \hat{C}_{2z} + \hat{C}_{2y} + \hat{C}_{2x} + \hat{\imath} + \hat{\sigma}_{xy} + \hat{\sigma}_{xz} + \hat{\sigma}_{yz}\right)$$
$$\hat{R}_{D_2} = \frac{1}{2}\left(\hat{I} + \hat{C}_{2xy} + \hat{C}_{2x\bar{y}} + \hat{C}_{2z}\right)$$

Coord	Definition	O_h irrep	Point group
S_1	$\frac{1}{\sqrt{3}}\hat{R}_{D_{2h}}\left(\delta x_1 + \delta y_1 + \delta z_1\right)$	a_{1g}	O_h
S_2	$\frac{1}{\sqrt{6}}\hat{R}_{D_{2h}}\left(-\delta x_1 - \delta y_1 + 2\delta z_1\right)$	$e_g\theta$	D_{4h}
S_3	$\frac{1}{\sqrt{2}}\hat{R}_{D_{2h}}\left(\delta x_1 - \delta y_1\right)$	$e_g\epsilon$	D_{2h}
S_4	$\frac{1}{2}\hat{R}_{D_2}\left(\delta x_1 - \delta y_1 + \delta x_2 + \delta y_2\right)$	$e_u\theta$	D_4
S_5	$\frac{1}{2}\hat{R}_{D_2}\left(\delta x_1 - \delta y_1 - \delta x_2 - \delta y_2\right)$	$e_u\epsilon$	D_{2d}
S_6	δx_{Bi}	$t_{1u}x$	C_{4v}
S_7	δy_{Bi}	$t_{1u}y$	C_{4v}
S_8	δz_{Bi}	$t_{1u}z$	C_{4v}

TABLE II: Combined distortions explored in this work that lead to low symmetry fields. Minimum Bi-O and O-O distances reached in the explored distortions, in Å.

Symmetry	Distortion	min d(Bi-O)	min d(O-O)
	g distortions		
O_h	S_1	2.44	2.82
$D_{4h(z)}$	S_2	2.55	2.71
D_{2h}	S_3	2.55	2.74
	u distortions		
D_4	S_4	2.55	2.94
D_{2d}	S_5	2.55	2.69
$D_{2(xy)}$	$S_4 = S_5$	2.55	2.71
$C_{4(z)}$	$S_2 = S_4$	2.56	2.73
$S_{4(z)}$	$S_2 = S_5$	2.56	2.73
$D_{2(x)}$	$S_3 = S_4$	2.55	2.71
$C_{2v(z)}$	$S_3 = S_5$	2.55	2.54
$C_{4v(z)}$	S_8	2.35	2.94
$C_{2v(yz)}$	$S_7 = S_8$	2.24	2.94
$C_{3v(xyz)}$	$S_6 = S_7 = S_8$	2.20	2.94
$C_{s(yz)}$	$S_7 = S_8/2$	2.24	2.94
C_1	$S_6 = S_7/2 = S_8/3$	2.14	2.94
$C_{4v(z)}$	$S_2 = S_8$	2.35	2.71
$C_{2v(y)}$	$S_2 = S_7$	2.34	2.71
$C_{s(yz)}$	$S_2 = S_7 = S_8$	2.21	2.77
C_1	$S_2 = S_6 = S_7 = S_8$	2.21	2.83
$C_{2v(z)}$	$S_3 = S_8$	2.35	2.74
$C_{2v(y)}$	$S_3 = S_7$	2.36	2.74
$C_{s(yz)}$	$S_3 = S_7 = S_8$	2.23	2.79
$C_{s(xz)}$	$S_3 = S_6 = S_8$	2.21	2.79
C_1	$S_3 = S_6 = S_7 = S_8$	2.21	2.84
$C_{4(z)}$	$S_4 = S_8$	2.35	2.96
$C_{2(y)}$	$S_4 = S_7$	2.33	2.95
C_1	$S_4 = S_7 = S_8$	2.21	2.95
C_1	$S_4 = S_6 = S_7 = S_8$	2.21	2.95
$C_{2v(z)}$	$S_5 = S_8$	2.35	2.74
$C_{s(yz)}$	$S_5 = S_7$	2.33	2.74
$C_{s(yz)}$	$S_5 = S_7 = S_8$	2.23	2.79
$C_{s(xz)}$	$S_5 = S_6 = S_8$	2.21	2.79
C_1	$S_5 = S_6 = S_7 = S_8$	2.21	2.84

Figure captions

FIG. 1: Atomic labels and cartesian axes of the BiO_8 moiety used in this work. Red arrows indicate the S_1 distortion defined in Table I.

FIG. 2: S_2 to S_8 basic distortions of the BiO_8 moiety chosen in this work as defined in Table I. S_1 is represented in Fig. 1.

FIG. 3: Bottom: Energies of the first excited state $^2P_{3/2}(1)$ (red lines) and second excited state $^2P_{3/2}(2)$ (blue lines) relative to the ground state $^2P_{1/2}$, ΔE, in O_h, D_{4h}, D_{2h}, D_4, and D_{2d} fields. Middle: First and second absorption electric dipole oscillator strengths, $f_{\text{abs}}(^2P_{1/2} \rightarrow^2 P_{3/2}(1))$ (full red lines) and $f_{\text{abs}}(^2P_{1/2} \rightarrow^2 P_{3/2}(2))$ (full blue lines); emitting state $^2P_{3/2}(1)$ radiative lifetime τ_{rad} (dashed red lines). Top: Distortions of the BiO_9 moiety leading to the fields.

FIG. 4: Energies of the first and second excited states relative to the ground state, ΔE; first and second absorption electric dipole oscillator strengths, f_{abs}; and emitting state radiative lifetime, τ_{rad}, in $D_{2(xy)}$, C_4, S_4, $D_{2(x)}$, and $C_{2v(z)}$ fields. See Fig. 3 caption for the meanings of the lines.

FIG. 5: Energies of the first and second excited states relative to the ground state, ΔE; first and second absorption electric dipole oscillator strengths, f_{abs}; and emitting state radiative lifetime, τ_{rad}, in $C_{4v(z)}$, $C_{2v(yz)}$, $C_{3v(xyz)}$, $C_{s(yz)}$, and C_1 fields. See Fig. 3 caption for the meanings of the lines.

FIG. 6: Energies of the first and second excited states relative to the ground state, ΔE; first and second absorption electric dipole oscillator strengths, f_{abs}; and emitting state radiative lifetime, τ_{rad}, in $C_{4v(z)}$, $C_{4(z)}$, $C_{s(yz)}$, and C_1 fields. See Fig. 3 caption for the meanings of the lines.

FIG. 7: Energies of the first and second excited states relative to the ground state, ΔE; first and second absorption electric dipole oscillator strengths, f_{abs}; and emitting state radiative lifetime, τ_{rad}, in $C_{2v(z)}$, $C_{2v(y)}$, $C_{s(yz)}$, and C_1 fields. See Fig. 3 caption for the meanings of the lines.

FIG. 8: Energies of the first and second excited states relative to the ground state, ΔE; first and second absorption electric dipole oscillator strengths, f_{abs}; and emitting state radiative lifetime, τ_{rad}, in $C_{4(z)}$, $C_{2(y)}$, and C_1 fields. See Fig. 3 caption for the meanings of the lines.

FIG. 9: Energies of the first and second excited states relative to the ground state, ΔE; first and second absorption electric dipole oscillator strengths, f_{abs}; and emitting state radiative lifetime, τ_{rad}, in $C_{2v(z)}$, $C_{s(yz)}$, and C_1 fields. See Fig. 3 caption for the meanings of the lines.

FIG. 10: Oxygen coordination of Bi^{2+} in a C_s Sr site of SrB_4O_7:Bi^{2+}. The Sr-O distances in the undoped host are: Sr-O_a 2.73 Å, Sr-O_b 2.47 Å, Sr-O_c 2.68 Å, Sr-O_d 2.79 Å, and Sr-O_e 2.90 Å [Ref. 39].

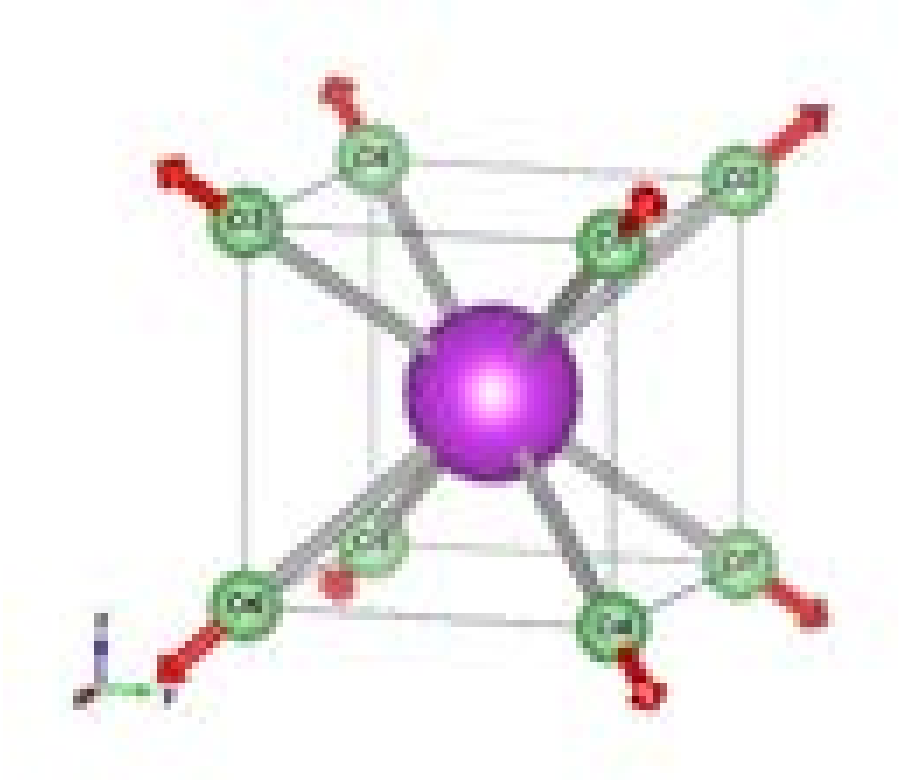

Figure 1. Seijo and Barandiarán

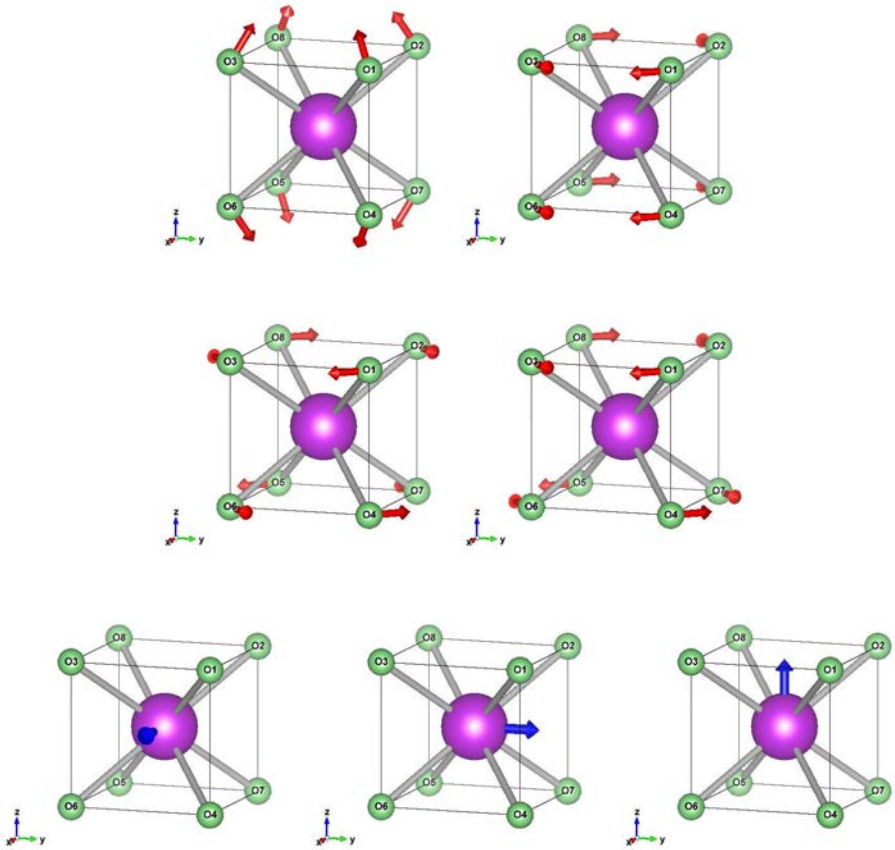

Figure 2. Seijo and Barandiarán

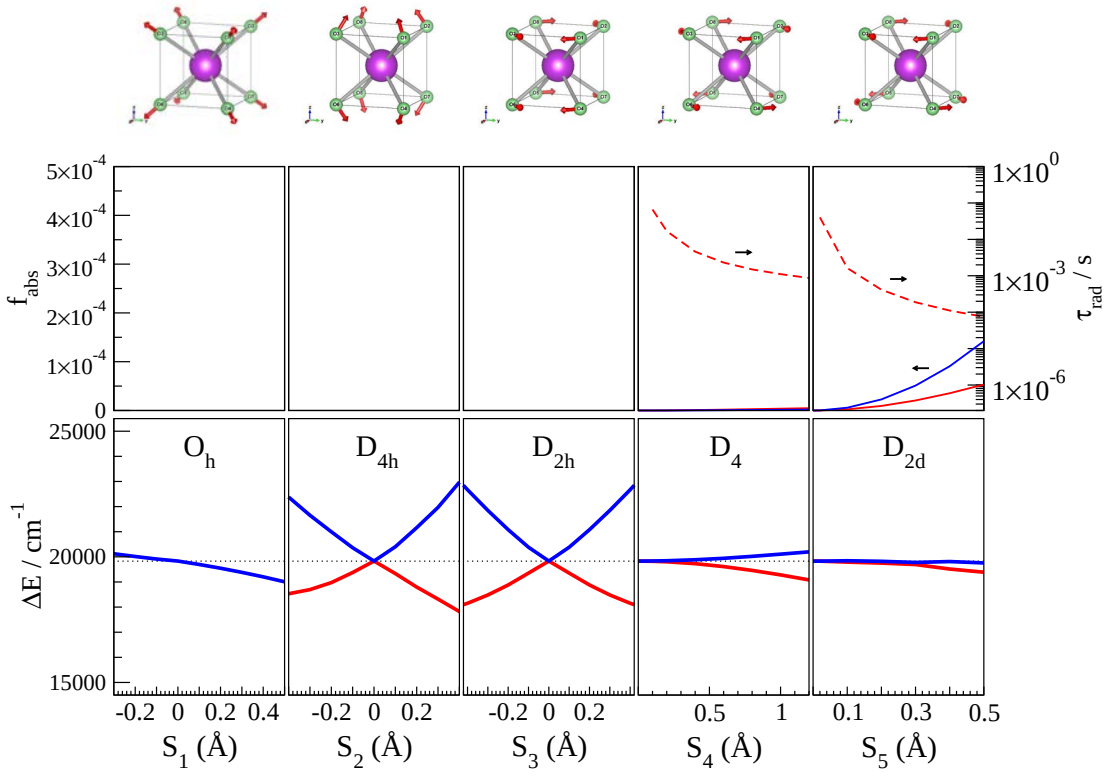

Figure 3. Seijo and Barandiarán

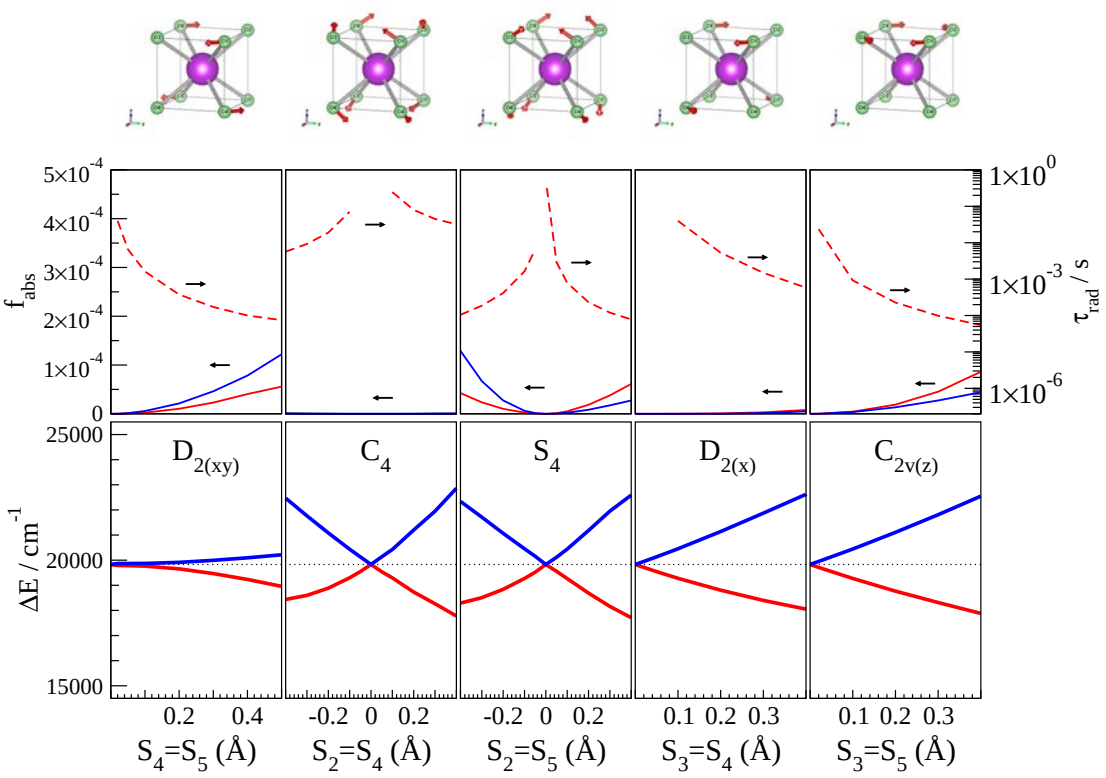

Figure 4. Seijo and Barandiarán

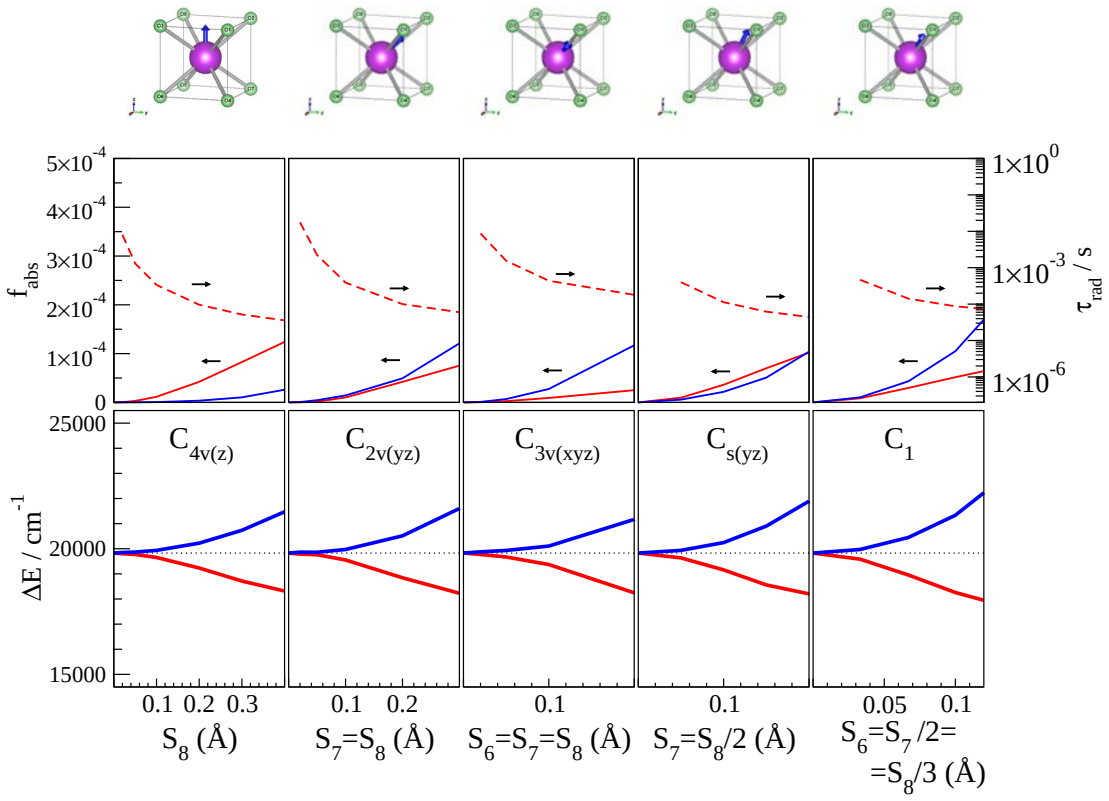

Figure 5. Seijo and Barandiarán

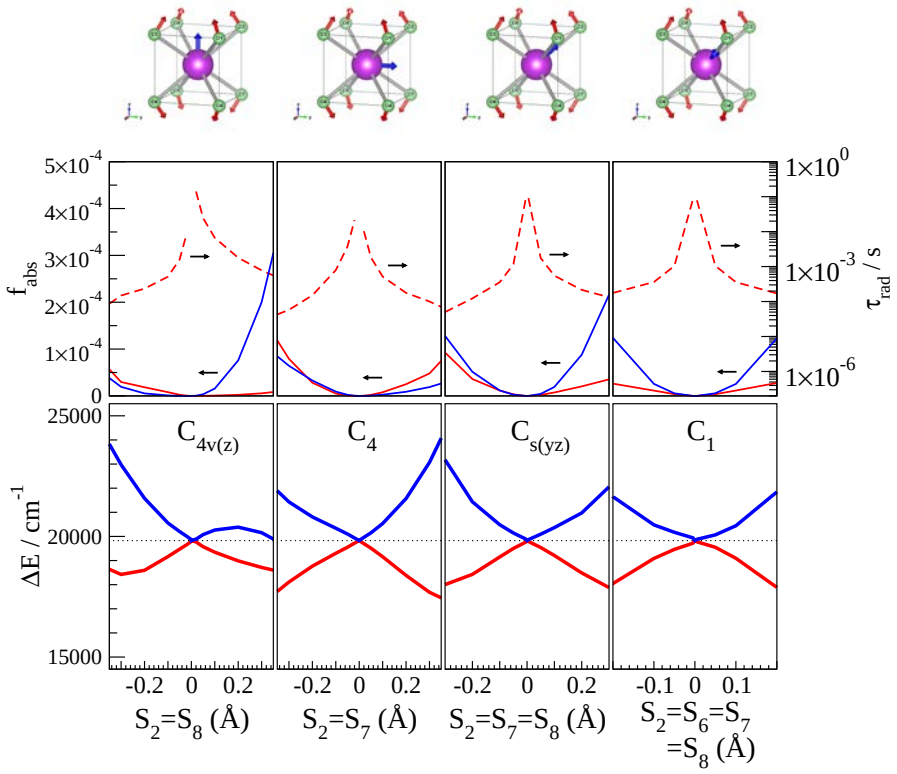

Figure 6. Seijo and Barandiarán

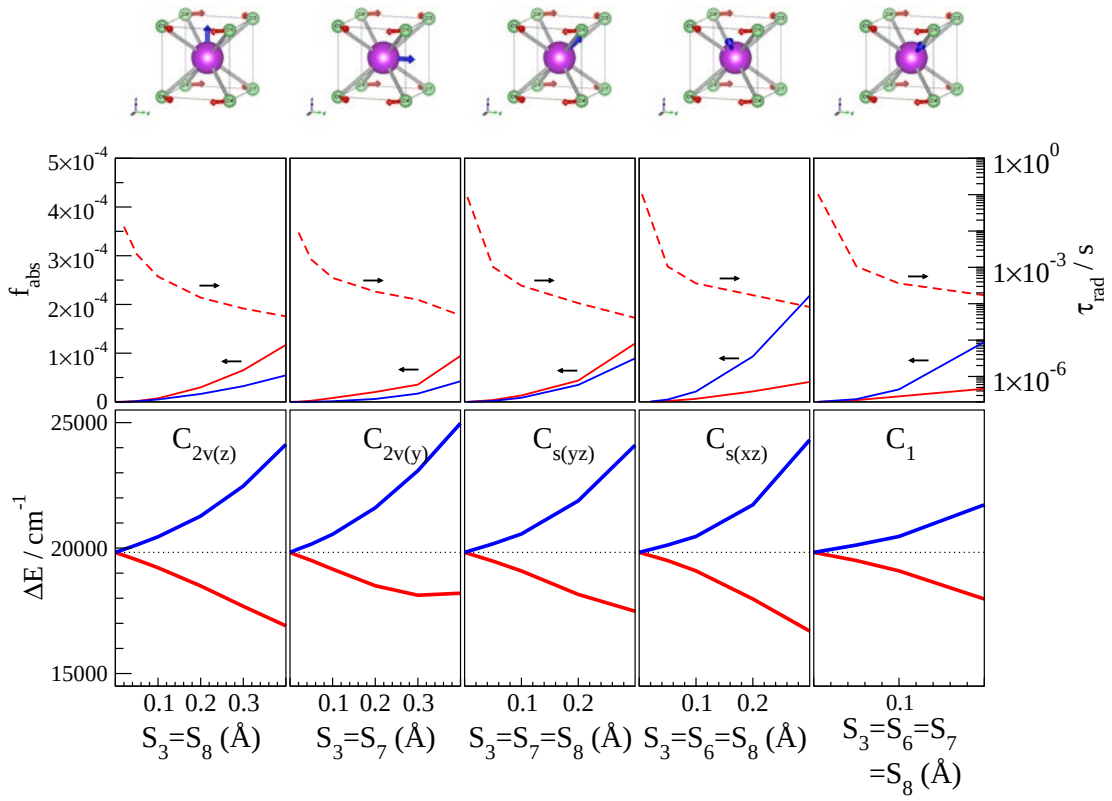

Figure 7. Seijo and Barandiarán

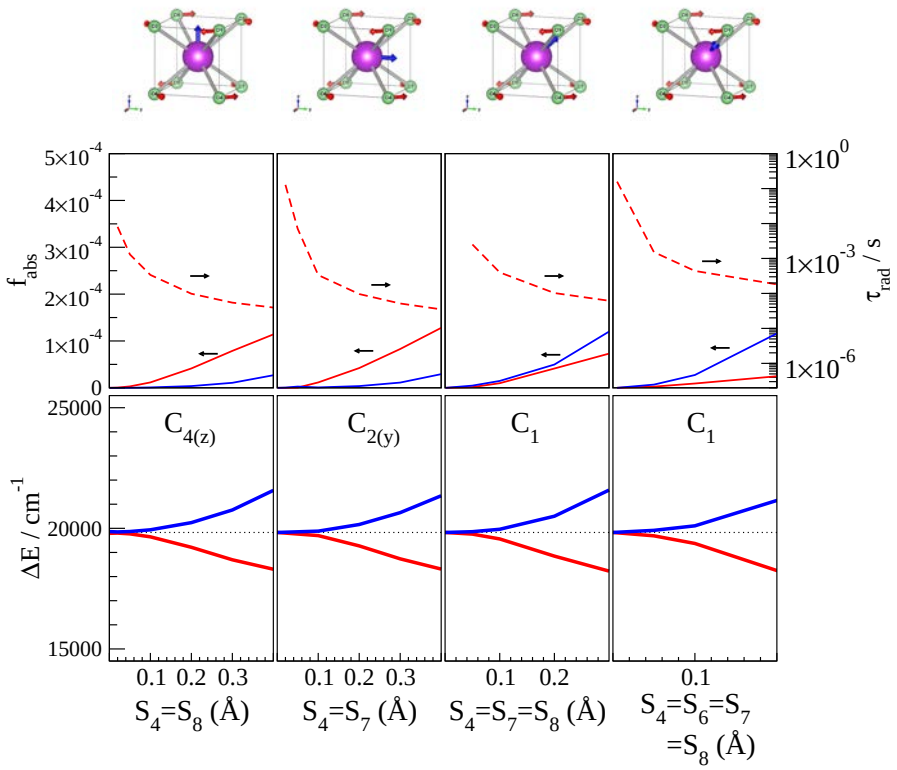

Figure 8. Seijo and Barandiarán

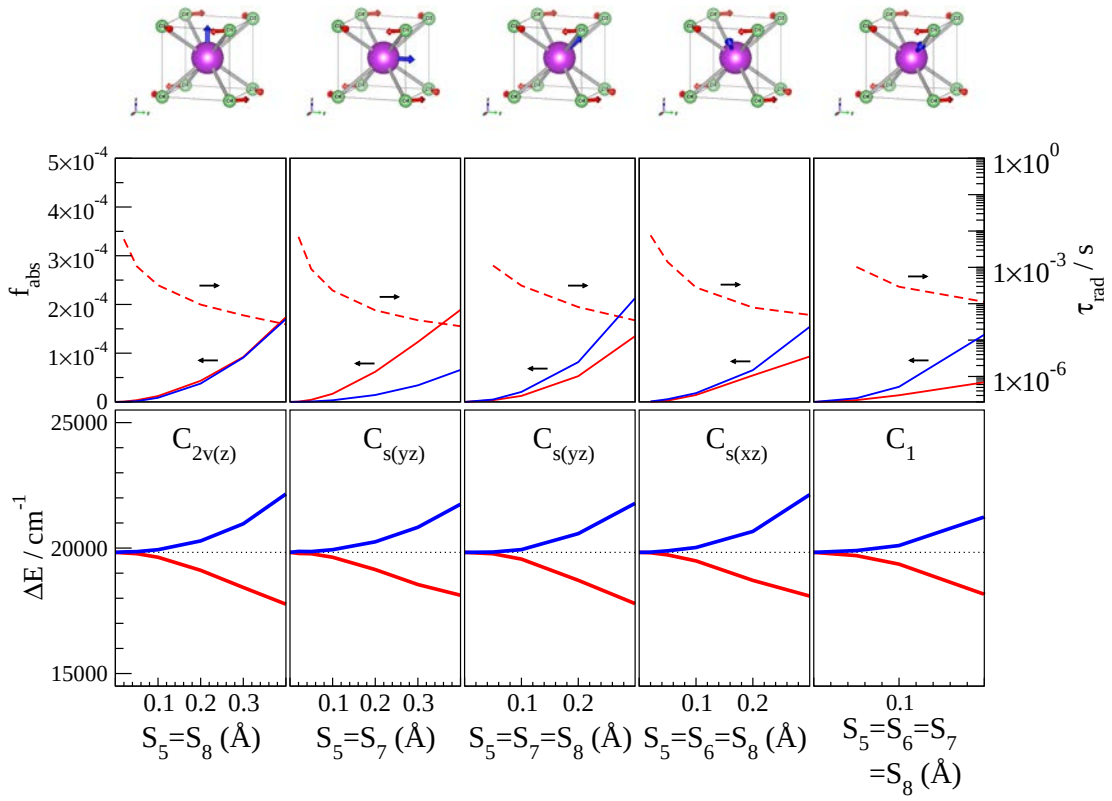

Figure 9. Seijo and Barandiarán

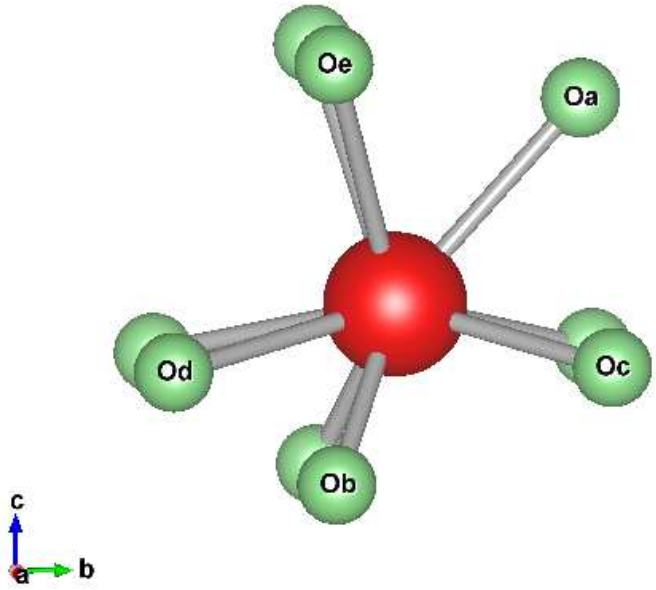

Figure 10. Seijo and Barandiarán